A New Toroidal-Meander Type Integrated Inductor With A Multilevel Meander Magnetic Core

Chong H. Ahn, *Member, IEEE,* and Mark G. Allen, *Member, IEEE*

Abstract—**A novel toroidal-meander type integrated (TMTI) inductor with a multilevel meander magnetic core has been designed, fabricated, and integrated onto a silicon wafer. In a conventional inductor, conductor wires are wound around magnetic cores. By switching the roles of conductor wire and magnetic core, i.e., by 'wrapping' a magnetic core around a conductor wire, the same effect can be realized in a planar geometry. This geometry has been implemented using multilevel metal interconnection schemes, by interlacing a meander planar conductor with a multilevel meander magnetic core. The total inductor size is 4 mm × 1.0 mm, the coil has 30 turns, and the magnetic material used was electroplated nickel(81%)-iron(19%) Permalloy. An inductance of 30 nH/mm^2 was achieved at a frequency of 5 Mhz. The fabrication sequence of this inductor structure is entirely compatible with post-processing of standard bipolar and CMOS circuitry, as well as the fabrication of multichip module substrates, thus enabling the integration of the inductor structure with control circuitry for applications such as filters, sensors, magnetic microactuators, and low-power voltage converters.**

Introduction

PLANAR inductors implemented on a chip have application in filters, sensors, dc/dc converters, and magnetic microactuators. Several different types of planar inductors have been proposed and fabricated to address these applications [1]–[9]. However, most planar inductive components have been fabricated without using a completely closed magnetic circuit [2], [3], [5]–[8], so that leakage flux from the inductor cannot be neglected. This can be a serious problem for integrating inductors and circuits on the same substrate for two reasons: first, magnetic flux interference with an integrated electronic circuit should be suppressed to reduce the magnetic noise in the circuits; and second, a high inductance per unit surface area is desirable in the small area, and any leakage flux produced does not contribute to the total inductance of the device. The conventional toroidal type inductor with a closed magnetic circuit can meet those requirements, since the wires wrapped around closed magnetic cores result in low leakage flux. Such structures have been fabricated using multilevel metal schemes to 'wrap' a wire around a magnetic core or air core, but tend to have relatively high resistance as two interconnect vias per turn are required to realize this device [9]. By interchanging the roles of the conductor wire and magnetic core in the conventional toroidal inductor, the same effect can be achieved; i.e., a multilevel magnetic core is 'wrapped' around a planar conductor. This structure has the advantage that a relatively short, planar conductor is used, thus reducing the total conductor resistance. In addition, this geometry has three advantages over the planar spiral-type geometry. First, the length of conductor wire necessary to achieve the same number of turns is shorter than that of spiral conductors, which results in smaller conductor series resistance. Second, since the magnetic cores are tightly linked with the conductor coils, the leakage flux is relatively low, resulting in relatively high inductance. Third, the magnetic core is produced on two levels, making it readily available for surface micromachining of movable core actuators, thus enabling magnetically-driven microactuation.

A schematic drawing of a section of the new integrated toroidal-meander type inductor, where toroidal refers to the core geometry and meander refers to the wrapping approach, is shown in Fig. 1. In the conventional toroidal inductor (Fig. 1(b)), the conductor lines are wrapped around a magnetic core to form an inductive component. Such structures can be realized using multilevel metal interconnect schemes to wrap conductor lines around magnetic materials (referred to here as a 'solenoid-bar type' inductive component). However, two problems arise from the solenoid-bar type inductor [9] in actual planar fabrication: first, electrical via contacts are used to connect the wrapped coils from layer to layer, which increases the total conductor resistance due to the via contact resistance; and second, the total length of coil is relatively long due to leaving adequate space for the multilevel coil interconnection vias, which also increases the total conductor resistance. Due to the extremely small cross section of conductor lines in any integrated inductor, the conductor line has a high electrical resistance even though it has a very short length. Thus, the reduction of this resistance while keeping the inductance relatively large is of extreme importance in integrated inductors operating at sub-GHz frequencies.

As mentioned earlier, an inductor can be realized by switching the roles of conductor and core as in Fig. 1(a); image 'wrapping' a magnetic core around a planar con-

Manuscript received November 20, 1992; revised April 30, 1993. This work was supported in part by the National Science Foundation under grant ECS-9117074.

The authors are with the School of Electrical and Computer Engineering, Microelectronics Research Center, Georgia Institute of Technology, Atlanta, GA 30332-0269.

IEEE Log Number 9213262.

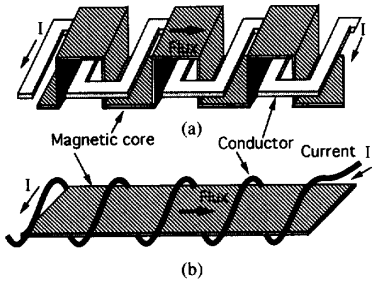

Fig. 1. Schematic diagrams of the toroidal-meander type integrated (TMTI) inductor with multilevel magnetic core and the more conventional toroidal or solenoid-bar type inductor. The structure of the two inductor schemes is analogous. (a) TMTI-inductor; (b) solenoid-bar type inductor.

ductor line. This geometry can also be realized using multilevel metal interconnect schemes, by interweaving a meander planar conductor with a multilevel meander magnetic core. This meander geometry has two advantages over the solenoid-bar type geometry. First, there are no electrical vias that add resistance to the conductor coil, since a planar meander conductor line is located on the simple surface without containing any electrical contacts. Second, the magnetic core is produced on two levels, making it readily available for surface micromachining of movable core actuators (i.e., integrated magnetic microactuators). The major disadvantage of the meander geometry is that the total length of magnetic core (and therefore the core reluctance) is slightly increased. To demonstrate the feasibility of this meander geometry, a new toroidal-meander type integrated (TMTI) inductor was designed and fabricated, whose scanning electron micrographs are shown in Fig. 2. A fully integrated magnetic microactuator has already been realized by incorporating surface micromachined moving parts as part of a magnetic circuit in the closed magnetic core [12].

Model

The meander inductor geometry is composed of meander-type conductor lines located on a simple plane and meander magnetic cores located on the multilevels as shown in Fig. 1(a). Since multilevel meander magnetic cores are interlaced through the center of each meander coil, the magnetic flux density at the center of each meander coil can be calculated by evaluating magnetic fields at the center points, which are generated from the current flowing through all meander conductor elements as shown in Fig. 3(a).

Consider two neighboring meander coils C1 and C2 carrying current I shown in Fig. 3(c). The self-inductance of meander coil C1 is defined as the magnetic flux linkage per unit current in the coil itself; that is,

$$L_{11} = \frac{\Lambda_{11}}{I}, \tag{1}$$

where Λ_{11} is the flux generated by C1 which links C1.

The mutual inductance between two meander conductor coils C1 and C2 is then the magnetic flux linkage with one circuit per unit current in the other, i.e.,

$$L_{12} = \frac{\Lambda_{12}}{I}, \tag{2}$$

where Λ_{12} is the flux generated by C1 which links C2.

By expanding this topology to all distributed meander conductor elements as shown in Fig. 3(b), the inductance can be calculated from the total flux linkage (both self and mutual flux linkage) as:

$$L = \frac{\Sigma\Lambda}{I}, \tag{3}$$

where $\Sigma\Lambda$ denotes the total flux linkage, which happens between the closed multilevel meander magnetic circuit

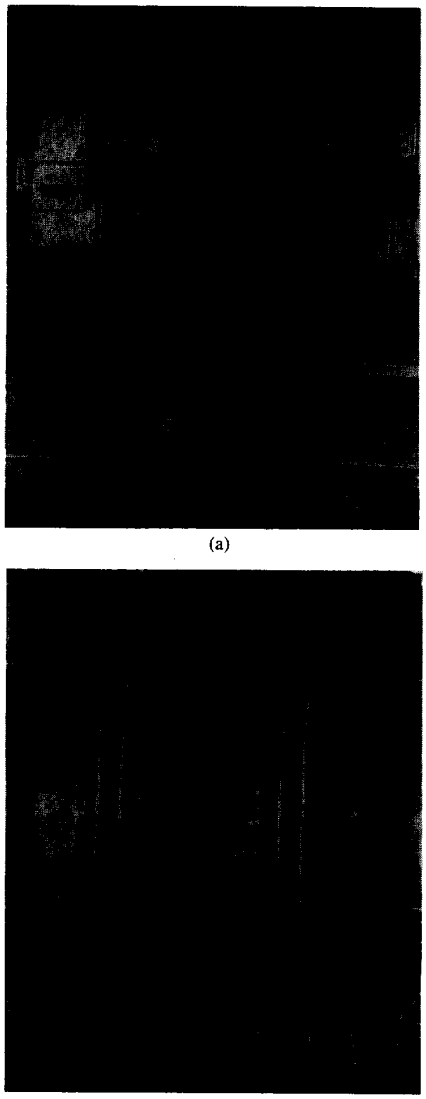

(a)

(b)

Fig. 2. Scanning electron micrographs of the fabricated TMTI-inductor: (a) view showing half of the TMTI-inductor structure; (b) detailed view of inductor elements.

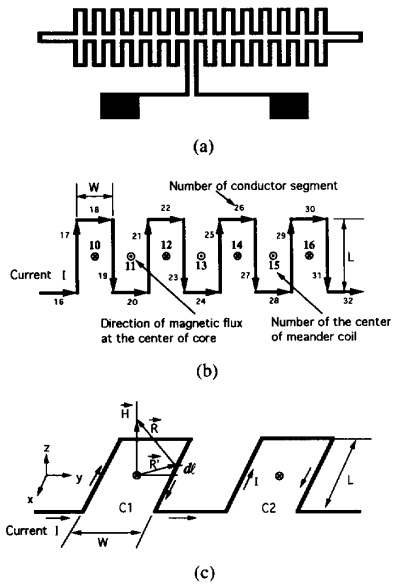

Fig. 3. Meander conductor models: (a) TMTI conductor geometry; (b) model of meander conductor including the direction of magnetic flux; (c) coordinate and meander elements for the Biot-Savart law calculation.

and the flux generated from the current flowing through all meander conductor elements. Note that this relation assumes that the material remains magnetically linear.

To determine the magnetic field at the center of a meander coil due to the current I in the coil, the Biot-Savart law can be invoked:

$$\vec{H} = \frac{I}{4\pi} \oint_c \frac{dl \times \hat{a}_R}{R^2}, \tag{4}$$

and applied to the meander conductor elements shown in Fig. 3(c), where $\hat{a}_R$ is the unit vector directed from the source point to the field point. The magnetic field at the center of a meander coil element is equal to the vector summation of the magnetic fields that are induced at the center by all elements of meander coil, satisfying the superposition principle. When a current of 1 mA flows through the meander conductor, Fig. 4 shows the distributed z-components of magnetic field that are generated by each meander conductor elements with respect to the center point of #13 meander coil in Fig. 3(b). Since magnetic cores with relatively large permeability are located at these centers, the magnetic flux, $B = \mu_0 \mu_r H$, will be concentrated mainly in these magnetic via cores. The z-components of the distributed magnetic flux at these centers are shown in Fig. 5. Although at the center of each meander coil, the vector direction of the z-component of the magnetic flux varies from point to point in the opposite direction, all fluxes of z-component in the magnetic circuit flow constructively through the multilevel meander core due to the core geometry. From the obtained total linkage flux and (3), the simulated inductance as a function of relative permeability is plotted in Fig. 6, where W and L of the simulated meander element shown in Fig.

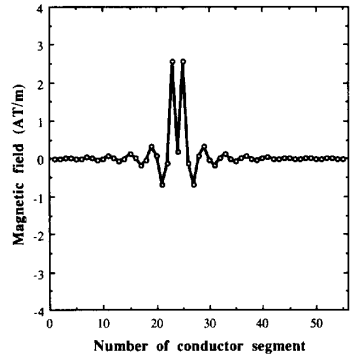

Fig. 4. The distribution of magnetic field with respect to the center of meander coil no. 13, which was generated from the distributed meander conductor elements with an assumed current of 1 mA flowing through the conductors. The number of meander conductor elements started from no. 1 at the element located between meander coil centers of no. 1 and no. 2. Thus, conductor elements nos. 23, 24, and 25 compose the meander coil surrounding meander core no. 13. The positive and the negative signs of magnetic field indicate the directions of magnetic field at Z-axis.

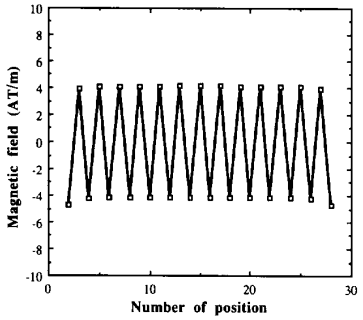

Fig. 5. Magnetic field distributions at the center of each meander coil with an assumed current of 1 mA flowing through the conductors. The positive and the negative signs of magnetic field indicate the directions of magnetic field at Z-axis.

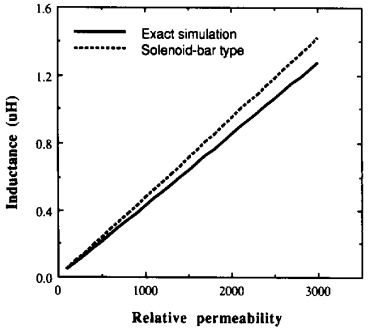

Fig. 6. Inductance obtained from (3) for the TMTI-inductor, and obtained from (5) for the analogous solenoid-bar type inductor.

3(b) are 120 μm and 500 μm respectively. Since the ratio of the via magnetic reluctance to that of the flat core part is negligibly small (2.3%), the contribution of the via magnetic reluctance is neglected in this simulation.

As shown in Fig. 1, the TMTI-inductor is analogous to

the simple schematic model of the more usual solenoid-bar type inductor. Once the validity of the analogy of both structures has been shown, the analysis of a TMTI-inductor can be made by using already well-developed analyses for the solenoid-bar type inductor. Thus, an analysis of an equivalent solenoid-bar type inductor will now be undertaken and compared with the results shown above.

The calculation of inductance for the solenoid-bar type structure depicted in Fig. 1(b) is very simple and more-or-less straightforward as reported earlier [1]. The inductance L of solenoid-bar type inductor structure (Fig. 1(b)) is expressed as:

$$L = \frac{\mu_0 \mu_r N^2 A_c}{l_c}, \tag{5}$$

where A_c is the cross-sectional area of film magnetic core, l_c is the length of closed magnetic core, and μ_0 and μ_r are the permeability of vacuum and the relative permeability of the magnetic core, respectively. To compare the inductance of the solenoid-bar type inductor structure (Fig. 1(b)) calculated from (5) with that of the TMTI-inductor, the analogous dimensions of the solenoid-bar type are chosen to have the same dimensions as the TMTI-inductor: inductor size of 4 mm × 1.0 mm; coil of 30 turns; μ_r of 500; and cross-sectional areas of magnetic core and conductor coil of 300 μm × 12 μm and 50 μm × 7 μm, respectively. A comparison of the inductance calculated from (5) for an analogous solenoid-bar type structure and the 'exact simulation' of the TMTI-inductor described above is shown in Fig. 6. The simulation results for the solenoid-bar type and TMTI-inductor are well matched, which ensures that the simple modeling technique used in the solenoid-bar type inductor is still useful in analyzing the TMTI-inductor.

The Q factor of an inductor can be expressed as:

$$Q = \frac{\omega L}{R} = \frac{\omega \mu_0 \mu_r N A_c A_w}{2(W + L)\rho l_c}, \tag{6}$$

where A_w is the cross section area of conductor, $2(W + L)$ is the length of one meander coil turn, and ρ is the resistivity of conductor material.

From (5) and (6), it is concluded that inductance and Q factor are linearly proportional to μ_r in the TMTI-inductor as well as in the conventional toroidal inductor due to the analogous structure in both inductors. Thus, the introduction of thin film magnetic core in the integrated inductor should improve its feasibility for IC applications. Eddy current losses in the magnetic core as well as skin depth effect in the conductor have been neglected in this calculation. This assumption should be justified since TMTI-inductors fabricated using IC technology will have cores and conductors which have geometries on the order of microns.

Fabrication

The fabrication process of this component is depicted in Fig. 7. The process starts with oxidized (0.6 μm) 2-in ⟨100⟩ silicon wafers as a substrate. Onto this substrate,

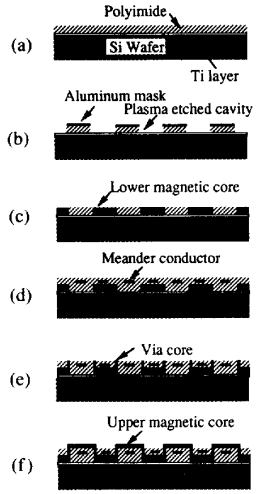

Fig. 7. Fabrication sequence of the TMTI-inductor: (a) polyimide deposition. (b) Dry-etching of plating molds. (c) Lower magnetic core plating. (d) Deposition and patterning of conductor. (e) Magnetic via plating. (f) Upper core plating.

2000 Å of titanium was deposited as an electroplating seed layer using dc sputtering. Polyimide (Dupont PI-2611) was then spun on the wafer to build electroplating molds for the bottom magnetic core. Four coats were accomplished to obtain a thick polyimide film. Each coat was cast at 3000 rpm, and soft baked for 10 min at 120°C before the application of the next coat. After deposition of all coats, the polyimide was cured at 350°C for 1 h in nitrogen, yielding an after-cure thickness of 12 μm. Holes were etched in this polyimide using a 5% CF_4/O_2 plasma etch and an aluminum hard mask until the titanium seed layer was exposed. The electroplating forms were then filled with nickel(81%)-iron(19%) Permalloy using standard electroplating techniques [10] and the nickel-iron electroplating bath described in Table I. To electroplate the bottom magnetic cores, electrical contact was made to the seed layer, and the wafers were immersed in the plating solution. During the electroplating, the solution was maintained at room temperature and a pH of approximately 2.7, and was stirred very slowly with a Teflon propeller blade. An applied current density of 5 mA/cm^2 resulted in a electroplating rate of 0.3–0.4 μm/minute. To insulate the bottom magnetic core from the conductor coil, polyimide was spin-coated (as above) at 4000 rpm, and hard-cured at 350°C for 1 h. Two different processes were used to make the conductor coils, one for a deposited aluminum conductor and one for a plated copper conductor. For the aluminum conductor, 7 μm of aluminum was dc sputtered onto the polyimide and patterned using conventional lithography and PAN (phosphoric-acetic-nitric) aluminum etching solution. For the plated copper conductor, copper was plated through a thick photoresist mold. A 2000 Å thick copper seed layer was deposited, and the copper plating mold was formed in 7 μm thick positive photoresist. The copper conductors were plated

TABLE I
COMPOSITION OF THE NICKEL–IRON AND COPPER ELECTROPLATING SOLUTIONS

Nickel-Iron Permalloy		Copper	
Component	Quantity (g/l)	Component	Quantity
$NiSO_4 \cdot 6H_2O$	200	$CuSO_4 \cdot 5H_2O$	1200 (g/l)
$FeSO_4 \cdot 7H_2O$	8	H_2SO_4	100 (ml/l)
$NiCl_2 \cdot 6H_2O$	5		
H_3BO_3	25		
Saccharin	3		

through the defined molds using standard electroplating techniques and the copper plating solution described in Table I. Note that the bottom magnetic core is electrically isolated from the plating solution during this step. Upon completion of the electroplating, the photoresist was removed with acetone, and the copper seed layer was etched in an HCl-based copper etching solution.

To insulate the conductor line and re-planarize the surface, more polyimide was deposited in multiple coats (as described above). Three coats of polyimide were deposited and cured as described above, yielding approximately 9 μm of polyimide. Via holes were then dry-etched through the polyimide layer between the meander conductors using 100% oxygen plasma and an aluminum hard mask. Upon completion of the via etch, the aluminum hard mask was removed. Because the botttom magnetic core was exposed to the oxygen plasma during dry etching, the surface of magnetic core was oxidized. To remove the oxide film, the exposed areas of the bottom magnetic cores were etched in a 2% hydrofluoric acid solution for 30 s. Contact was then made to the bottom magnetic core, and the vias were filled with nickel–iron using the electroplating bath and conditions described previously. Upon completion of the electroplating, the magnetic vias were coated with a single layer of polyimide spun on the wafer at 5000 rpm and cured as described above.

The top magnetic core was then plated over the magnetic vias, completing the magnetic circuit. To electroplate top cores, an evaporated nickel seed layer was defined between the magnetic vias using a liftoff technique. After construction of the photoresist plating mold, top magnetic cores were plated using the electroplating conditions described above. Bonding pads were then opened through polyimide layers for the electrical test by using the via etch process sequence described earlier. Optionally, to remove the titanium plating seed layer located underneath the polyimide, the structure was dry etched to the bottom, and the titanium was then selectively dry etched using a 90% CF_4/O_2 plasma. It should be noted that removal of the magnetic core plating base was not required for successful device performance. Fig. 8 shows the side view of the multilevel meander inductive component after this optional removal step has been carried out. Note the magnetic via connecting the top and bottom cores in the meander topology. Finally, samples were

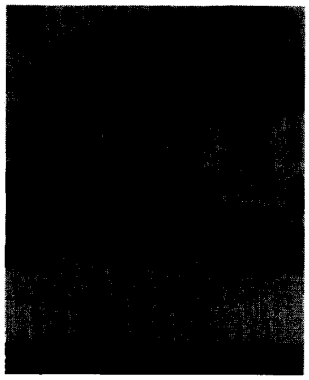

Fig. 8. Scanning electron micrograph of the side wall of magnetic via after removal of encapsulating polyimide.

Fig. 9. TMTI-inductors mounted in a ceramic package, where two TMTI-inductors are shown.

diced into chips for bonding and test. The diced TMTI-inductor chip was mounted in the ceramic package as shown in Fig. 9.

EXPERIMENTAL RESULTS AND ANALYSIS

The dimensions of the fully fabricated TMTI-inductor shown in Fig. 2 are as follows: the total inductor size is 4 mm × 1.0 mm; the coil has 30 turns; μ_r is 500; and the cross sectional areas of the magnetic core and the conductor coil are 300 μm × 12 μm and 50 μm × 7 μm, respectively. The magnetic material used was electroplated nickel(81%)-iron(19%) Permalloy [10], and the conductor material used was sputter-deposited aluminum.

The inductance of the device was measured using an HP-4192A impedance analyzer. The measured inductance values were plotted in Fig. 10, which shows a fairly flat response through a frequency of 10 Mhz (approximately the limit of the impedance analyzer used). At a frequency of 5 Mhz, an inductance of 30 nH/mm^2 was achieved. The inductance calculated from the model of conventional toroidal inductor at $\mu_r = 500$ (a typical value for the core material used) was 0.22 μH from Fig. 6, but the measured inductance at low frequencies around 20 Khz was 0.2 μH at the same relative permeability, giving 0.02 μH discrepancy between them.

To generate an easy axis in the nickel-iron Permalloy film and thereby increase the permeability, an external magnetic field of 100–500 gauss should be applied to the parallel direction of easy axis during the electroplating. However, no external magnetic field was applied in this fabricated device. Thus, if the relative permeability of

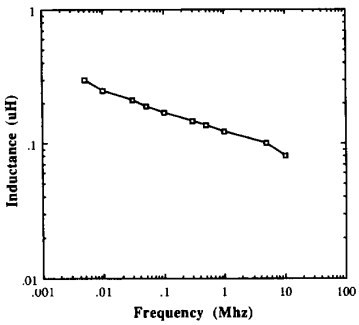

Fig. 10. Measured inductance of the TMTI-inductor as a function of frequency.

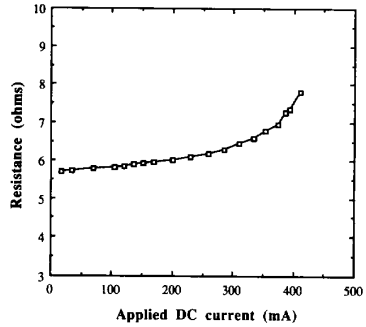

Fig. 11. Resistance of meander conductor from the measured slope of voltage-current curve, applying DC current through conductors using Tectronix 370A programmable curve tracer.

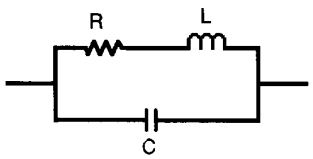

Fig. 12. The equivalent circuit of TMTI-inductor used to analyze circuit parameters.

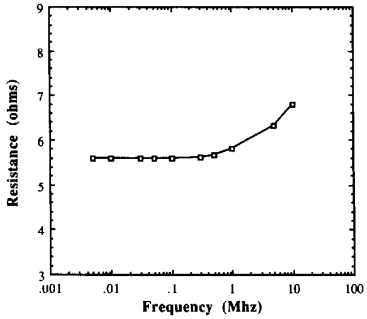

Fig. 13. The resistance of the inductor obtained from the measured impedance and phase angle as the function of frequency using the equivalent circuit of TMTI-inductor.

magnetic film can be increased to 5000 by applying an external magnetic field [11], several μH of inductance will be available with this structure.

When this inductor is used as an inductive component for a power device such as an integrated dc/dc converter, the heat dissipation capability of the inductor will limit the maximum current flowing through conductors. By applying dc current through the inductor coils using an Tectronix 370A programmable curve tracer, coil resistance was estimated from the slope of the V-I curve. These results are plotted in Fig. 11. Using the equation of resistance-temperature for the conductor, the temperature of conductor could be calculated from the measured resistance, which was reached to 50°C at 250 mA. This indicates that the meander film conductor permits high current density. For instance, the maximum recommended current density of conventional inductor [13] in the macro scale at 50°C has been reported as 5×10^2 A/cm^2. In the TMTI-inductor, it was verified that the attainable maximum current density ranged from 5×10^4 A/cm^2 to 5×10^5 A/cm^2. These values are 10^2-10^3 times larger than the values in the macro scale, which probably represent the large difference in surface-to-volume ratios of conductors in the macro and micro scale, or the easy dissipation of the generated heat in the conductor because most meander conductors are exposed on or near the surface of the wafer.

To obtain the circuit parameters of the inductor, an equivalent circuit was assumed as shown in Fig. 12, and the resistance and stray capacitance of the inductor were derived from the measured impedance and phase as a function of frequency using equivalent circuit analysis. From this analysis, the stray capacitance was shown to be in the *p*F region, and also shown to have a negligibly small effect over the frequency ranges used. The effect of the inductance falloff at higher frequencies shown in Fig. 10 is due almost entirely to the dependence of the permeability of the iron-nickel core on frequency, and has been confirmed using other test structures. The variation of resistance as a function of measured frequency is shown in Fig. 13.

With knowledge of the measured inductance and the derived resistance as a function of frequency, the Q value of the device can be estimated from (6). The Q value at a frequency of 10 Mhz is approximately unity. Several approaches such as increased conductor thickness (to lower the series resistance) or increased core permeability could be taken to increase the Q-factor. For example, it was described earlier in this section that μ_r as high as 5000 could be achieved by applying an external field during the plating of the magnetic film. If this value can be achieved, the Q factor may be expected to also increase, which may be high potentially resulting in a high enough Q factor for low-power dc-dc converter applications [14].

Conclusion

A new integrated toroidal-meander type of inductor with multilevel meander magnetic core (the TMTI-inductor) has been realized on a silicon wafer using micromachining techniques. Because of the nature of its geometry,

this inductor has the following characteristics: 1) small conductor resistance due to smaller length of conductor line; 2) low leakage flux due to the tight linkage of both conductor and magnetic core; 3) flexibility of the fabrication of movable surface magnetic microactuators due to the already-existing multilevel magnetic cores. For an inductor size of 4 mm × 1.0 mm with 30 turns of meander coil around a closed magnetic core, the achieved inductance was about 0.2 μH (μ_r = 500), showing fairly flat variations through 10 Mhz. The measured DC resistance of the aluminum meander conductor was 5.6 ohms. It was verified that the simulation behavior of the TMTI-inductor is similar to the more conventional toroidal type or solenoid-bar type inductor. The calculated inductance matches well with the measured inductance. The TMTI-inductor implemented on a chip or as an integral part imbedded in the interconnections of a multichip module can play a role as an inductive component in realizing magnetic integrated circuits or modules such as filters, sensors, dc/dc converters, and magnetic microactuators.

Acknowledgment

The donation of the polyimides used in this work by the DuPont corporation is also gratefully acknowledged. Microfabrication was carried out at Microelectronics Research Center of Georgia Tech. Valuable technical discussions with Mr. Young W. Kim, Dr. A. Bruno Frazier, and Dr. Bizhan Rashidian of Georgia Tech, as well as Professor Martin Schmidt of MIT, are greatly appreciated.

References

[1] R. F. Soohoo, "Magnetic thin film inductor for integrated circuit application," *IEEE Trans. Magn.*, vol. MAG-15, pp. 1803-1805, 1979.

[2] K. Kawabe, H. Koyama, and K. Shirae, "Planar inductor," *IEEE Trans. Magn.*, vol. MAG-20, pp. 1804-1806, 1984.

[3] O. Oshiro, H. Tsujimoto, and K. Shirae, "A novel miniature planar inductor," *IEEE Trans. Magn.*, vol. 23, pp. 3759-3761, 1987.

[4] H. M. Greenhouse, "Design of planar rectangular microelectronic inductors," *IEEE Trans. Parts, Hybrids, and Packaging*, vol. PHP-10, no. 2, pp. 101-109, 1974.

[5] W. A. Roshen, "Effect of finite thickness of magnetic substrate on planar inductors," *IEEE Trans. Magn.*, vol. MAG-26, pp. 270-275, 1990.

[6] H. Matsuki, H. Miyzawa, K. Murakami, and T. Yamamoto, "Miniaturization limit of a cloth inductor," *J. Appl. Phys.*, vol. 63, no. 8, pp. 3394-3396, 1988.

[7] K. Shirakawa, K. Yamaguchi, M. Hirata, T. Yamaoka, F. Takeda, K. Murakami, and H. Matsuki, "Thin film cloth-structured inductor for magnetic integrated circuit," *IEEE Trans. Magn.*, vol. MAG-26, pp. 2262-2264, 1990.

[8] M. Yamaguichi, M. Matsumoto, H. Ohzeki, and K. I. Arai, "Fabrication and basic characteristics of dry-etched micro inductors," *IEEE Trans. Magn.*, vol. MAG-26, pp. 2014-2016, 1990.

[9] S. Kawahito, Y. Sasaki, M. Ashiki, and T. Nakamura, "Micromachined solenoids for highly sensitive magnetic sensors," Digest of 6th International Conference on Solid-State Sensors and Actuators, pp. 1077-1080, San Francisco, 1991.

[10] M. E. Henstock and E. S. Spencer-Timms, "The composition of thin electrodeposited alloy films with special reference to nickel-iron," *Proc. 6th International Metal Finishing Conference*, pp. 179-185, 1963.

[11] R. L. Anderson, E. E. Castellani, P. M. McCaffrey, and L. T. Romankiw, "Method for treating magnetic alloy to increase the magnetic permeability," United States Patent #4,003,768.

[12] C. H. Ahn and M. G. Allen, "A fully integrated surface micromachined magnetic microactuator with a multilevel meander magnetic core," *IEEE J. Microelectromech. Syst.*, vol. 2, no. 1, pp. 15-22, 1993.

[13] C. W. T. McLyman, *Transformer and Inductor Design Handbook*, New York: Marcel Dekker, Inc., pp. 84-89, 1988.

[14] C. H. Ahn, Y. J. Kim, and M. G. Allen, "A fully integrated micromachines toroidal inductor with a nickel-iron magnetic core (the switched DC/DC boost converter application," Transducers, 7th International Conference on Solid-State Sensors and Actuators, pp. 70-73. Yokohama, Japan, June 7-10, 1993.

Chong H. Ahn (M'93) received the B.S. degree in electrical engineering from Inha University, South Korea, in 1980, the M.S. degree in electrical engineering from Seoul National University, South Korea, in 1983, and the Ph.D. degree in electrical and computer engineering from the Georgia Institute of Technology in 1993.

He is currently a postdoctoral fellow at the Microelectronics Research Center, School of Electrical and Computer Engineering, Georgia Institute of Technology, Atlanta, GA. His research interests include the development, design, fabrication, and characterization of fully integrated microsensors and microactuators; micromachined planar inductive components; planar magnetic micromotors; and integrated dc/dc converters, using microfabrication technologies.

Mark G. Allen (M'90) received the B.A. degree in Chemistry, the B.S.E. degree in Chemical Engineering, and the B.S.E. degree in Electrical Engineering from the University of Pennsylvania in 1984, the S.M. degree from the Massachusetts Institute of Technology in 1986, and the Ph.D. degree from MIT in 1989.

Since 1989 he has been Assistant Professor in the School of Electrical Engineering at Georgia Institute of Technology. Dr. Allen's research include micromachining fabrication technology, micro-optomechanical systems, and materials issues in micromachined structures and electronic packages.

Dr. Allen is a member of the editorial board of the *Journal of Micromechanics and Microengineering*.